Sensitive detection of Cre-mediated recombination using droplet digital PCR reveals Tg(*BGLAP*-Cre) and Tg(*DMP1*-Cre) are active in multiple non-skeletal tissues.

Krishnakali Dasgupta PhD[1,2], Samantha Lessard BS[1], Steven Hann PhD[1], Megan A. Fowler BA[1], Alexander G. Robling PhD[3], Matthew L. Warman MD[1,2]

1. Orthopedic Research Laboratories, Department of Orthopedic Surgery, Boston Children's Hospital, Boston, MA

2. Department of Genetics, Harvard Medical School, Boston, MA

3. Indiana University School of Medicine, Indianapolis, IN

Correspondence to:

Matthew L. Warman, M.D.

Orthopedic Research Labs, EN250

Boston Children's Hospital

320 Longwood Avenue

Boston, MA 02115

Phone: 617-919-2371

Email: matthew.warman@childrens.harvard.edu

Supplementary Materials: Supplementary Figures 1 - 7; Supplementary Tables 1 and 2

This is the author's manuscript of the article published in final edited form as:

Dasgupta, K., Lessard, S., Hann, S., Fowler, M. E., Robling, A. G., & Warman, M. L. (2021). Sensitive detection of Cre-mediated recombination using droplet digital PCR reveals Tg(BGLAP-Cre) and Tg(DMP1-Cre) are active in multiple non-skeletal tissues. Bone, 142, 115674. https://doi.org/10.1016/j.bone.2020.115674

Abstract

In humans, somatic activating mutations in *PIK3CA* are associated with skeletal overgrowth. In order to determine if activated PI3K signaling in bone cells causes overgrowth, we used Tg(*BGLAP*-Cre) and Tg(*DMP1*-Cre) mouse strains to somatically activate a disease-causing conditional *Pik3ca* allele (*Pik3ca*^{H1047R}) in osteoblasts and osteocytes. We observed Tg(*BGLAP*-Cre);*Pik3ca*$^{H1047R/+}$ offspring were born at the expected Mendelian frequency. However, these mice developed cutaneous lymphatic malformations and died before 7 weeks of age. In contrast, Tg(*DMP1*-Cre);*Pik3ca*$^{H1047R/+}$ survived and had no cutaneous lymphatic malformations. Assuming that Cre-activity outside of the skeletal system accounted for the difference in phenotype between Tg(*BGLAP*-Cre);*Pik3ca*$^{H1047R/+}$ and Tg(*DMP1*-Cre);*Pik3ca*$^{H1047R/+}$ mice, we developed sensitive and specific droplet digital PCR (ddPCR) assays to search for and quantify rates of Tg(*BGLAP*-Cre)- and Tg(*DMP1*-Cre)-mediated recombination in non-skeletal tissues. We observed Tg(*BGLAP*-Cre)-mediated recombination in several tissues including skin, muscle, artery, and brain; two CNS locations, hippocampus and cerebellum, exhibited Cre-mediated recombination in >5% of cells. Tg(*DMP1*-Cre)-mediated recombination was also observed in muscle, artery, and brain. Although we cannot preclude differences in phenotype between mice with Tg(*BGLAP*-Cre)- and Tg(*DMP1*-Cre)-mediated PIK3CA activation being due their inducing Cre-recombination at different stages of osteoblast differentiation, differences in recombination at non-skeletal sites of are the more likely explanation. Since unanticipated sites of recombination can affect the interpretation of data from experiments involving conditional alleles, we recommend ddPCR as a good first step for assessing efficiency, leakiness, and off-targeting in experiments that employ Cre-mediated or Flp-mediated recombination.

Key words: Mouse, Osteoblasts, Osteocytes, Osteocalcin, BGLAP, Cre-recombination, PIK3CA

Introduction

Congenital Lipomatous Overgrowth with Vascular, Epidermal and Skeletal anomalies (CLOVES) syndrome is a non-heritable congenital overgrowth syndrome caused by somatic activating mutations in *PIK3CA,* the gene which encodes a catalytic subunit of the enzyme phosphatidyl-inositol-3 phosphate kinase (PI3K)[2]. Intracellular signaling via class 1 PI3K enzymes normally occurs in response to ligand-dependent activation of receptor tyrosine kinases, including the vascular endothelial growth factor receptor and insulin-like growth factor receptor [3]. Effector proteins, that function downstream of PI3K signaling, include the AKT (Ak strain transforming) and mTOR (mammalian target of rapamycin) proteins, which are involved in cell proliferation and survival[4]. Also in this signaling pathway is the enzyme PTEN (phosphatase and tensin homologue deleted on chromosome 10), which is a phosphatase that reverses the action of PI3K[5].

Among the intriguing features of CLOVES syndrome, and other disorders within the PIK3CA-related overgrowth spectrum, is localized overgrowth of limbs or digits that are composed of cells having endodermal, mesodermal, and ectodermal origins[6,7]. Because CLOVES is caused by somatic mutation, it seems unlikely that an early embryonic mutation would affect multiple cell lineages all ending up in a single limb or digit. More likely, is that a somatic mutation in the progenitor of one cell type drives overgrowth of other tissues via paracrine signaling. The importance of PI3K signaling in osteoblasts was inferred from studies that used Tg(*BGLAP*-Cre) to inactivate *Pten* in osteoblasts, which led to increased bone mass[8]. Here, we used Tg(*BGLAP*-Cre) and Tg(*DMP1*-Cre) to conditionally activate a gain-of-function *Pik3ca* allele in osteoblasts and osteocytes.

Mice with Tg(*BGLAP*-Cre)- *and* Tg(*DMP1*-Cre)-mediated activation of *Pik3ca* had very different phenotypes, but no appendicular overgrowth. The difference in phenotypes is likely due to the transgenic Cre drivers causing Cre-mediated recombination at sites other than bone. Since many experiments utilize conditional alleles, and unanticipated sites of recombination can

affect data interpretation, we developed a droplet digital PCR (ddPCR) method that is sensitive, specific, rapid, and cost-effective for determining sites and levels of Cre-mediated recombination.

Materials and Methods

Mouse strains and husbandry

The Institutional Animal Care and Use Committee at Boston Children's Hospital approved all animal experiments. Mice with Tg(*BGLAP*-Cre)[9], Tg(*DMP1*-Cre)[10], *R26*^{mTmG} [11], and *R26*$^{l\text{-}s\text{-}lLacZ}$ [12] alleles were purchased from the Jackson Laboratory (JAX stock #s 019509, 023047, 007676, and 003474). *Pik3ca*^{H1047R} mice[13] were obtained from Dr. Wayne Phillips at the Peter McCallum Institute in Melbourne Australia. Cells from *Pik3ca*^{H1047R} mice express wild-type PIK3CA until Cre-recombination causes expression of a constitutively active form of this enzyme. Mice with *Prg4*^{GT} alleles were created and maintained in our lab[14], and are available from the Jackson Lab (JAX stock # 025740).

Hemizygous male Tg(*BGLAP*-Cre) mice were crossed with female *Pik3ca*$^{H1047R/H1047R}$, *R26*$^{mTmG/mTmG}$, *R26*$^{l\text{-}s\text{-}lLacZ/l\text{-}s\text{-}lLacZ}$, or *Prg4*$^{GT/GT}$ mice. Hemizygous Tg(*DMP1*-Cre) males were crossed with *Pik3ca*$^{H1047R/+}$ mice. Offspring were genotyped as previously described and, after weaning, maintained with same sex littermates. Tg(*BGLAP*-Cre);*Pik3ca*$^{H1047R/+}$ offspring were monitored daily because their clinical phenotype warranted early euthanasia. Some Tg(*BGLAP*-Cre);*Pik3ca*$^{H1047R/+}$ offspring and offspring from the other crosses were euthanized at 14, 18, 21, 24, 27, 28, 34, or 60 days of age for tissue collection. Tg(*DMP1*-Cre);*Pik3ca*$^{H1047R/+}$ offspring displayed no overt phenotype and were euthanized at 3 months of age.

Sample collection and DNA extraction

Twenty-one-day-old mutant (Tg(*BGLAP*-Cre);*Pik3ca*$^{H1047R/+}$) and control (*Pik3ca*$^{H1047R/+}$) mice were given anesthesia using 2% isoflurane and subjected to retro-orbital blood collection using heparinized and non-heparinized capillary tubes. Blood samples were sent to the small animal core lab at Boston Children's Hospital for automatic blood cell counting and biochemical analyses, respectively.

Twenty-one-day-old mutant (Tg(*BGLAP*-Cre);*Pik3ca*$^{H1047R/+}$, Tg(*BGLAP*-Cre);*R26*$^{mTmG/+}$ and Tg(*BGLAP*-Cre);*Prg4*$^{GT/+}$), and control (*Pik3ca*$^{H1047R/+}$, *R26*$^{mTmG/+}$ and *Prg4*$^{GT/+}$) mice were euthanized. Thirty different tissues, including calvarial bone, 5th lumbar vertebra, cerebral cortex, dorsal cerebellum, midbrain representing the junction of the cerebral cortex and superior colliculi, skin overlying the 5th lumbar vertebra, tongue, clavotrapezius (neck) muscle, femoral artery, ovary, testis, liver and kidney were immediately collected and stored at -20°C. Approximately 20 mg of each tissue was used to extract genomic DNA using the Qiagen Blood and Tissue DNA extraction kit. Extracted DNA was stored in water, quantified using Nanodrop technology, and kept at -20°C. Separate femoral and vertebral bones were also dissected, cleaned of soft tissue, fixed for 1 week in 4% paraformaldehyde (PFA), and then transferred to 70% ethanol. We collected 11 different tissues from Tg(*DMP1*-Cre);*Pik3ca*$^{H1047R/+}$, Tg(*DMP1*-Cre);*Pik3ca*$^{+/+}$, *Pik3ca*$^{H1047R/+}$, and wild-type littermates. Femora, skulls, and vertebral bones were also collected from 3-month-old Tg(*DMP1*-Cre);*Pik3ca*$^{H1047R/+}$ and Tg(*DMP1*-Cre);*Pik3ca*$^{+/+}$ mice.

Histologic sectioning, LacZ staining, and Immunohistochemistry

Heads from Tg(*BGLAP*-Cre);*R26*$^{l\text{-}s\text{-}lLacZ/+}$ and *R26*$^{l\text{-}s\text{-}lLacZ/+}$ littermates were recovered from P14, P34, and P60 animals. After the skin was gently removed the specimens were fixed in 4% PFA for 10 minutes followed by 2 washes in 1X phosphate buffered saline (PBS). The specimens were then equilibrated sequentially in 15% Sucrose/PBS overnight and 30% Sucrose/PBS

overnight at 4^{O}C, embedded in OCT, frozen on dry ice, cryosectioned at 10 µm and stored at -80°C. Other heads from Tg(BGLAP-Cre);Pik3ca$^{H1047R/+}$, Tg(*DMP1*-Cre);Pik3ca$^{H1047R/+}$ and control mice were stored in Bouin's fixative prior to embedding, sectioning, and hematoxylin and eosin staining by the rodent histology core at Harvard Medical School.

LacZ staining was performed by thawing sections at room temperature for 10 min, immersing the slides for 10 min each in: 0.2% glutaraldehyde/2mM $MgCl_2$/PBS, then 1X PBS, then 2mM $MgCl_2$/PBS, and then 2mM $MgCl_2$/PBS/0.01%DOC/0.02%NP-40. All steps were performed in solutions kept on ice. Slides were then immersed in 0.1% X-Gal/2mM $MgCl_2$/0.01% DOC/02% NP-40/1.05% Potassium HexacyanoFerrate(II)/0.825% Potassium Ferricyanide (III)/PBS, wrapped in aluminum foil and incubated in the dark for at least 8 hours at 37°C. Slides were then rinsed in PBS, fixed in 4% PFA for 2 hours at room temperature, rinsed again in PBS and then counterstained for 2 minutes with Nuclear Fast Red stain solution. After gently rinsing in water, the slides were dehydrated sequentially with ethanol (50% -1 min, 70% - 1min, 100% - 1 min X 2) followed by xylene (2 min X 3). After mounting in Permount (Fisher Scientific) and cover-slipping, the slides were then dried for two more days.

Immunodetection of Phospho-mTor was performed on P18 6µm coronally sectioned Tg(*BGLAP*-Cre);*Pik3ca*$^{H1047R/+}$ and *Pik3ca*$^{H1047R/+}$ heads that were prepared for cryosectioning as described above and immediately fixed in ice-cold acetone for 5 min and air dried. Endogenous peroxidase activity was quenched using 3% hydrogen peroxide in methanol for 20 min. After 3 washes with Tris buffered saline (TBS), a rabbit monoclonal anti-Phospho-mTOR(Ser2448) antibody (Cell Signaling #2976) at 1 to 350 dilution using the TSA kit's TNB buffer (Perkin Elmer) was overlayed onto the sections and incubated overnight at 4°C. After 3 washes with TBS/0.5% Tween20, a horse radish peroxidase (HRP)-conjugated goat anti-rabbit secondary antibody (Jackson Immunoresearch) at dilution 1 to 400 in TNB buffer was added for 30 min at room temperature. After 3 washes with TBS/0.5% Tween20, amplification of signal was done

using the TSA kit with biotinylated tyramide and streptavidin HRP following the manufacturer's recommendation. Diaminobenzidine was used as the chromophore with hematoxylin counterstaining.

Tartrate resistant acid phosphatase (TRAP) staining of long bone sections was performed as previously described[15].

Photomicrographs were obtained using a Nikon Eclipse 80i microscope at 40X and 100X magnification, and captured with a Nikon digital sight DSRi1 camera using the NIS Elements software. Quantitative histomorphometry for osteoblasts and osteoclasts is reported using standard nomenclature[16].

Bone µCT and fluorochrome labeling of mineralizing tissue

Femoral and vertebral bone µCT imaging, and fluorochrome labeling with fluorescence imaging, were performed as previously described[17].

Droplet digital PCR

Droplet digital PCR was performed as previously described[1]. Briefly, DNA was diluted to a concentration of ~ 10 ng/µl, and ~ 30 ng of DNA was used in each reaction. Supermix for Probes mastermix (BioRad) was used following the manufacturer's recommendations. PCR was performed using Eppendorf ep gradient S machines, nanodroplets were created using an automatic droplet generator, amplimer containing droplets were counted with a QX200 sample reader, and data were analyzed using Quantasoft software (all from BioRad). The primer pairs and probes described below were purchased from IDT (Coralville, IA) and were used to amplify and quantify the number conditional and recombined alleles. At least 1000 amplimer containing droplets per tissue sample per animal were created in order to measure Cre-mediated recombination.

For the *Pik3ca*^{H1047R} allele: Two PCR primers 19For-25:CAAGGGAGAGGAATGGTAAGG and mut20R-*Bam*H1: CAACTCAGGCATGCCGGATCCCAA generated a 719 bp amplimer for from the conditional allele and a 265 bp amplimer from the recombined allele. The conditional allele was detected using a 5HEX/CGAAGTTATTTGTTAGACCCTT/3IABkFQ probe, while the recombined allele was detected using a 56-FAM/CGAAGTTATGTTAACTTGTTAGACC/3IABkFQ probe. The PCR reaction was 95°C/10mins, followed by 40 cycles of 94°C/30s; 56°C/60s; 72°C/60s, followed by 98°C/10mins until cooling to 4°C. The cycling ramp time was 1.2s/°C.

For the *R26*^{mTmG} allele (Figure 2): Three PCR primers, p9104: CCATGTTCATGCCTTCTTCTT, p9102: TGATGACCTCCTCTCCCTTG, and p9107:TGCTCACGGATCCTACCTTC generated a 238 bp amplimer for the conditional allele and a 331 bp amplimer for the recombined allele. The conditional allele was detected using a 5HEX/CGAAGTTATATTAAGGGTTCCGGATCC/3IABkFQ probe, while the recombined allele was detected using a 56-FAM/TCCGGATCATCACCGCGGATGGGT/3IABkFQ probe. The PCR reaction was the same as above, except the primer annealing temperature was 55°C.

For the *Prg4*^{GT} allele: Three PCR primers 5'loxp-f: TGTGTTGACAGTCGACATATAACTTCG, insert-r:TCTAGGACAAGAGGGCGAGA, and wt-r:AAGGAAGAGAGAGCATTGAAGG generated a 304 bp amplimer for the conditional allele and a 226 bp amplimer for the recombined allele. The conditional allele was detected using a 5HEX/TCGGTTCCTCTTCCCATGAATTCCA/3IABkFQ probe, while the recombined allele was detected using a 56-FAM/TCCCCTCGAGGGACCTAATAACTTCGT/3IABkFQ probe. The PCR reaction was the same as above, except the primer annealing temperature was 58°C.

Results

<u>Tg(*BGLAP*-Cre)-mediated activation of PI3K signaling causes early lethality in mice.</u>

In order to generate mice in which PI3K activity is constitutively active in osteoblasts and osteocytes, hemizygous male Tg(*BGLAP*-Cre) mice were bred to *Pik3ca*$^{H1047R/H1047R}$ females. *Pik3ca*^{H1047R} produces wild-type protein until Cre-mediated recombination induces mutant protein expression. Equal numbers of Tg(*BGLAP*-Cre)*;Pik3ca*$^{H1047R/+}$ and *Pik3ca*$^{H1047R/+}$ offspring were born. Pups did not appear phenotypically different during the 1st week of life and had similar long bone histology (Supplementary Figure 1). By ~ 2 weeks of age, Tg(*BGLAP*-Cre)*;Pik3ca*$^{H1047R/+}$ mice were smaller (Figure 1A) and less active than their *Pik3ca*$^{H1047R/+}$ littermates, and they had swelling over the surface of their skulls. Histologic examination revealed enormous lymphatic channels in the skin overlying the head (Figure 1B) and blood clots were detected between the skin and calvarium by necropsy. Tg(*BGLAP*-Cre)*;Pik3ca*$^{H1047R/+}$ mice died spontaneously or required euthanasia before 7 weeks of age (Figure 1D). No other abnormalities of major organs including heart, lung, liver, kidney, intestine and brain were observed on gross or microscopic inspection. The presence of clotted blood and the knowledge that the bone microenvironment can affect hematopoiesis[18-20], prompted us to perform blood profiles on Tg(*BGLAP*-Cre)*;Pik3ca*$^{H1047R/+}$ mice when they were 3 weeks of age; numbers of white blood cells, red blood cells, platelets, and bleeding times were normal (data not shown). Since bone cells have been reported to directly and indirectly regulate systemic energy metabolism and ion homeostasis[21,22], we also measured serum glucose, electrolytes, calcium, phosphorus, albumin, total protein, alkaline phosphatase, urea, and creatinine levels in 3-week-old Tg(*BGLAP*-Cre)*;Pik3ca*$^{H1047R/+}$ and control (*Pik3ca*$^{H1047R/+}$) littermates, and saw no differences (data not shown). Lastly, since Tg(*BGLAP*-Cre);*Pten*$^{fl/fl}$ mice were previously found to develop increasing bone mass with aging[8], we examined bone mass in Tg(*BGLAP*-Cre)*;Pik3ca*$^{H1047R/+}$ mice using µCT and fluorochrome labeling. These animals had less femoral, calvarial, and vertebral bone than their control littermates (Figure 1C, Supplementary Figures 2 and 3, Supplementary Table 1). Calcein labeling indicated bone mineralization was still occurring in P24 mutant and control animals. However, the proliferating and hypertrophic

chondrocyte zones in the growth plates of the mutant mice appeared smaller than those of their control littermates (Supplementary Figure 3). TRAP staining for osteoclasts and quantification of osteoclast and osteoblast numbers revealed no difference between Tg(*BGLAP*-Cre);*Pik3ca*$^{H1047R/+}$ and *Pik3ca*$^{H1047R/+}$ littermates at P0 (data not shown), but a significant reduction in the number of osteoblasts and osteoclasts in Tg(*BGLAP*-Cre);*Pik3ca*$^{H1047R/+}$ compared to *Pik3ca*$^{H1047R/+}$ littermates at P27 (Supplementary Figure 4).

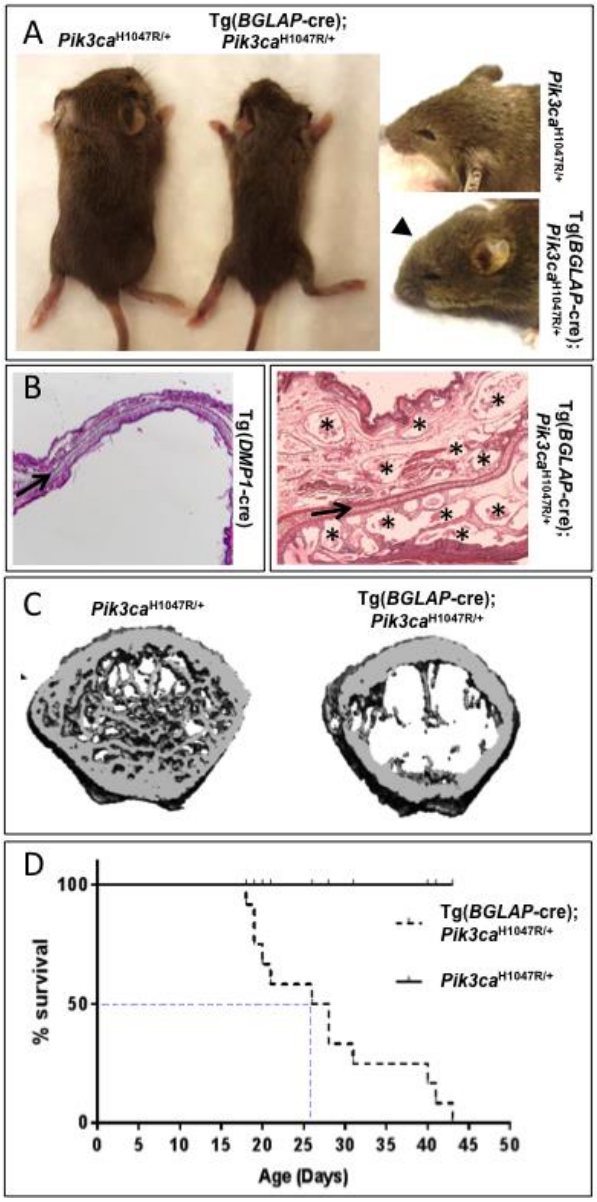

Figure 1. Impaired growth, reduced bone mass, and early lethality in Tg(*BGLAP*-Cre);*Pik3ca*$^{H1047R/+}$ mice.
(A) Photographs comparing 2-week-old *Pik3ca*$^{H1047R/+}$ and Tg(*BGLAP*-Cre);*Pik3ca*$^{H1047R/+}$ littermates. Note Tg(*BGLAP*-Cre);*Pik3ca*$^{H1047R/+}$ mice are smaller and have swelling over the cranium (arrowhead). **(B)** Representative 40X photomicrographs of hematoxylin and eosin stained sections through the external ears of control Tg(*DMP1*-Cre) and mutant Tg(*BGLAP*-Cre);*Pik3ca*$^{H1047R/+}$ mice. Ear cartilage is indicated with arrows. Note the multiple enlarged lymphatic channels (asterisks) between the cartilage and the epidermis in the mutant mice **(C)** Transverse µCT reconstructions of the distal femur of 4-week-old *Pik3ca*$^{H1047R/+}$ and Tg(*BGLAP*-Cre);*Pik3ca*$^{H1047R/+}$ littermates. Note the Tg(*BGLAP*-Cre);*Pik3ca*$^{H1047R/+}$ mouse bone has few trabeculae. **(D)** Kaplan-Meier plot following *Pik3ca*$^{H1047R/+}$ and Tg(*BGLAP*-Cre);*Pik3ca*$^{H1047R/+}$ mice (N = 13 animals/genotype). Note all Tg:*BGLAP*-Cre;*Pik3ca*$^{H1047R/+}$ mice died before 7 weeks of age.

Tg(*DMP1*-Cre)-mediated activation of PI3K signaling is not lethal.

To exclude the possibility that lymphatic swelling over the skull was a direct effect of Pik3ca activity in bone cells, we studied Tg(*DMP1*-Cre);*Pik3ca*$^{H1047R/+}$ mice. These animals did not die early, had normal skin, and had thicker skull bones than control mice (Supplementary Figure 5). Mean midshaft femur cortical bone volume was also significantly higher in the Tg(*DMP1*-Cre);*Pik3ca*$^{H1047R/+}$ mice compared to littermate controls (1.22 mm^2 vs. 0.96 mm^2, $p < 0.01$, n = 3 mice/genotype).

Tg(*BGLAP*-Cre) recombines conditional (i.e., floxed) alleles in multiple tissues.

Because early lethality in Tg(*BGLAP*-Cre)*;Pik3ca*$^{H1047R/+}$ mice was not clearly attributable to osteoblast dysfunction, we looked for Cre-mediated recombination in other tissues where constitutive activation of PI3K signaling would be detrimental. Studies have reported that activating the *Pik3ca*^{H1047R} allele in endothelial cells causes venous[23] and lymphatic[24] malformations. Activation in the central nervous system can cause early lethality or seizures[25], and global activation in adult mice causes death from hypoglycemia within several weeks[26]. We collected multiple tissues from 3-week-old Tg(*BGLAP*-Cre)*;Pik3ca*$^{H1047R/+}$ mice to look for Tg(*BGLAP*-Cre) mediated recombination outside of the skeletal system. Age matched littermates (i.e., *Pik3ca*$^{H1047R/+}$) that lack the *BGLAP*-Cre transgene were controls for testing the specificity of the assay. We used ddPCR, which is a sensitive tool for detecting low levels of somatic mosaicism[1,27,28]. Thus, if the Tg(*BGLAP*-Cre) were active in non-bone tissues, ddPCR would detect “off-target” recombination. Recombination rates for 8 different tissues from 3-week-old Tg(*BGLAP*-Cre)*;Pik3ca*$^{H1047R/+}$ mice are presented in Table 1**.**

Table 1

	Tg(*BGLAP*-cre); *Pik3ca*$^{H1047R\ flox/+}$		Tg(*BGLAP*-cre); *R26*$^{mTmG/+}$		Tg(*BGLAP*-cre); *Prg4*$^{GT/+}$		Tg(*DMP1*-cre); *Pik3ca*$^{H1047R/+}$	
	Mean (%)	SD	Mean (%)	SD	Mean (%)	SD	Mean (%)	SD
Calvaria	**9.8**	1.2	**27.6**	0.5	**19.8**	3.8	**21.1**	2.1
	23.9	0.8	**15.6**	2.0	**25.8**	0.1	**29.7**	1.6
	14.1	0.4			**21.2**	2.7	**17.5**	1.6
Vertebra	**14.5**	2.8	**8.3**	0.3	**14.27**	4.74	**11.7**	1.8
	12.4	0.5	**6.1**	0.4	**8.05**	2.19	**17.4**	0.8
	11.4	0.3			**10.33**	0.91	**12.0**	0.5
Midbrain	**6.66**	0.4	**0.7**	0.1	**9.9**	0.5	**11.2**	5.4
	1.34	0.2	**6.9**	1.1	**2.1**	3.2	**3.2**	1.5
	4.70	0.7			**7.7**	0.1	**3.8**	0.5
Cerebellum	**2.58**	0.8	**5.8**	0.9	**1.1**	0.5	**1.1**	0.3
	7.03	1.1	**0.6**	0.3	**5.1**	1.6	**0.5**	0.3
	5.01	1.1			**1.1**	0.1	**0.9**	0.0
Skin	**8.1**	0.5	**0.6**	0.0	**1.8**	0.4	**0.1**	0.0
	7.5	0.4	**0.5**	0.2	**1.5**	0.2	**0.5**	0.3
	10.5	0.23			**1.3**	0.4	**0.2**	0.1
Tongue	**3.4**	0.3	**0.7**	0.4	**1.1**	0.1	**10.2**	2.1
	5.4	0.4	**0.6**	0.0	**1.2**	0.2	**12.1**	0.4
	3.3	0.8			**1.3**	0.2	**17.9**	3.7
Aorta	**3.2**	0.5	0.4	0.3	**0.6**	0.1	**1.8**	0.1
	2.9	0.3	0.1	0.0	**0.5**	0.1	**2.7**	0.4
	8.1	0.5			**0.5**	0.2	**10.7**	1.8
Liver	0.1	0.0	0.0	0.0	0.0	0.0	0.0	0.0
	0.0	0.0	0.0	0.1	0.0	0.0	0.0	0.0
	0.0	0.0			0.0	0.1	0.0	0.0

Table 1 legend: Tg(*BGLAP*-Cre)-mediated recombination in 3-week-old mice and Tg(DMP1-Cre)-mediated recombination in 3-month-old mice.
Recombination frequencies were measured by ddPCR. DNA was recovered from the same sites in 2 or 3 mice (each row represents 1 mouse) having 1 of 3 different (*Pik3ca*^{H1047R}, *R26*^{mTmG}, or *Prg4*^{GT}) floxed alleles (each column represents one of the conditional alleles). All ddPCR assays were performed in triplicate; the mean recombination frequency ± standard deviation (SD) for each experiment is shown. No conditional or recombined droplets were detected when either water or wild-type mouse DNA was used as template (Supplementary Table 2). Additionally, no recombined droplets were detected when DNA from mice with conditional alleles alone (i.e., no Tg(*BGLAP*-Cre) allele) was used as template (Supplemental Table 1); since a minimum of 1000 amplimer-containing droplets from each tissue was analyzed, these results indicate the ddPCR assays are highly specific. When DNAs from mice with a conditional allele and the Tg(*BGLAP*-Cre) transgene were assayed, recombination was detected in several but not all tissues. In this table, representative examples are shown. Recombined allele frequencies greater than 0.5%, which exceeds a conservative threshold we previously employed for calling true positives[(1)], are bolded. Tissue-specific differences in recombination frequency between animals with the same genotype may reflect biologic variation or sampling error due to the tissues having diverse cell types that are mosaic for the recombined allele. Of note, similar levels of recombination were detected in the midbrains and cerebellums of floxed mice, irrespective of the conditional allele. In contrast, the Cre-recombination frequency was higher in skin, tongue, and femoral artery from Tg(*BGLAP*-Cre); *Pik3ca*$^{H1047R/+}$ mice, which is consistent with cells containing mutant PI3K having a proliferative advantage in these tissues. Nevertheless, in skin and in tongue Tg(*BGLAP*-Cre) still caused recombination at rates of ~ 1-in-200 to ~ 1-in-75, in mice with *R26*^{mTmG}, or *Prg4*^{GT} alleles, respectively. Tg(*DMP1*-Cre) also caused recombination in several non-skeletal tissues.

Neither water controls, nor DNA from wild-type mice or from mice with only the *Pik3ca*^{H1047R} allele had evidence of recombination [Supplementary Table 2], indicating this ddPCR assay is highly specific. Calvarial and vertebral DNA from Tg(*BGLAP*-Cre)*;Pik3ca*$^{H1047R/+}$ mice contained recombined alleles. Importantly, several other tissues from Tg(*BGLAP*-Cre)*;Pik3ca*$^{H1047R/+}$ mice also contained recombined alleles. For example, recombined alleles were observed in ~ 9% of skin cells, ~ 5% of midbrain cells, ~ 5% of cerebellar cells, and ~ 5% of clavotrapezius muscle cells (Table 1).

In addition to causing CLOVES syndrome and other malformation disorders when arising during embryogenesis[1], the p.H1047R mutation in *PIK3CA* is a common somatic mutation that arises in cancer[29]. Thus, recombination in non-skeletal tissues of Tg(*BGLAP*-Cre)*;Pik3ca*$^{H1047R/+}$ mice could be very low, with the abundance of recombined cells increasing over time because they have a proliferative advantage. To test this hypothesis, we bred the Tg(*BGLAP*-Cre) into two other mouse strains, in which Cre-mediated recombination would not give recombined cells a proliferative advantage. This would enable us to differentiate tissues that have appreciable amounts of Tg(*BGLAP*-Cre) "off-target" expression from those that have very low levels of "off-target" expression that appear high because of increased cell proliferation.

Hemizygous male Tg(*BGLAP*-Cre) mice were bred to female mice homozygous for *Prg4*^{GT} or *R26*^{mTmG}. The *Prg4*^{GT} allele is a loss-of-function allele at the lubricin locus that restores lubricin expression after Cre-recombination[14]. Presence or absence of lubricin should have no effect on cell proliferation in brain, muscle, and skin. The *R26*^{mTmG} allele ubiquitously expresses membrane-bound tomato fluorescent protein (mTFP) until Cre-recombination changes expression to membrane bound green fluorescent protein (mGFP)[11]. This allele is commonly used to visualize sites of Cre-mediated recombination using fluorescence microscopy (https://www.jax.org/strain/007676), since the switching from mTFP to mGFP is not thought to alter cell proliferation or viability.

Droplet digital PCR data derived from DNA extracted from 3-week-old Tg(*BGLAP*-Cre)*;R26*$^{mTmG/+}$ (Figure 2) and Tg(*BGLAP*-Cre) *;Prg4*$^{GT/+}$ mice are included in Table 1.

Age-matched littermates lacking the Cre transgene served as negative controls. As with the *Pik3ca*^{H1047R} ddPCR assay, these ddPCR assays are highly specific since no recombined amplimer-containing droplets were observed when DNA from mice with the conditional allele alone was used as ddPCR template [Supplementary Table 2]. Importantly, midbrain and cerebellar cells from Tg(*BGLAP*-Cre)*;R26*$^{mTmG/+}$ and Tg(*BGLAP*-Cre)*;Prg4*$^{GT/+}$ mice continued to demonstrate significant levels of Cre-mediated recombination (Table 1). Also, although lower than in mice with the conditional *Pik3ca*^{H1047R} allele, Cre-mediated recombination still occurred in skin and muscle of mice with *Prg4*^{GT} or *R26*$^{mTmG/+}$ alleles. Hence, the Tg(*BGLAP*-Cre) allele expresses catalytically active Cre-recombinase in multiple non-skeletal tissues.

We also looked for non-skeletal expression of Cre-recombinase in 3-month-old Tg(*DMP1*-Cre);Pik3ca$^{H1047R/+}$ mice (Table 1). Interestingly, recombination rates exceeding 10% were observed in muscle, and rates exceeding 5% were seen in artery and midbrain. However, in contrast to Tg(BGLAP-Cre);Pik3ca$^{H1047R/+}$ mice which had recombination rates > 6% in skin at 3-weeks-old, Tg(*DMP1*-Cre);Pik3ca$^{H1047R/+}$ mice had only 0.2% recombination

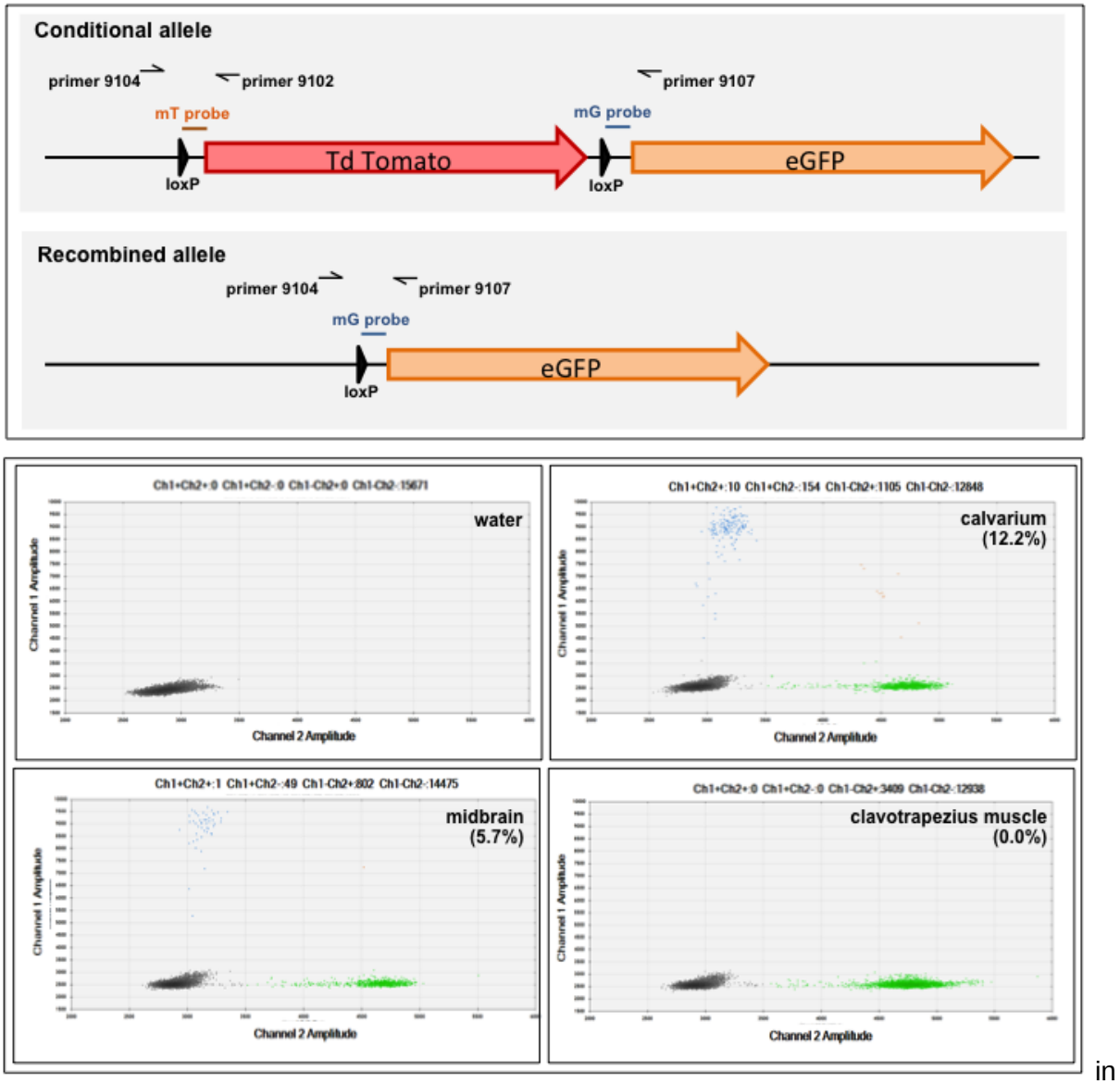

in

Figure 2. The ddPCR assay for the *R26*^{mTmG} allele.
(Upper panels) Schematic diagrams (not to scale) of the conditional and Cre-recombined mTmG alleles. The locations of the primers and probes used in the ddPCR assay are indicated. Note in the conditional allele, primers 9104 and 9107 are too far apart to produce PCR product that is detected using the mT or mG probe. **(Lower panels)** ddPCR assay results obtained using DNA extracted from calvarium, midbrain, and clavotrapezius muscle in a 20-day-old Tg(*BGLAP*-Cre);*R26*$^{mTmG/+}$ mouse. Droplets lacking amplimers are pseudocolored black. Droplets containing amplimers from the conditional allele (channel 2 positive) are pseudocolored green, while droplets containing amplimers from the recombined allele (channel 1 positive) are pseudocolored blue. The percentage of amplimer-containing droplets (conditional or recombined) that have a recombined allele is indicated beneath each tissue. No amplimer-containing droplets were observed in the water control. In neck muscle, 3409 droplets containing amplimer from the conditional allele were observed. In midbrain, 49

skin at 3-months-old.

Tg(*BGLAP*-Cre) expression localizes to subsets of cells within the central nervous system.

Droplet digital PCR indicated that Tg(*BGLAP*-Cre) is active in the CNS. To determine which cells had expressed the Tg(*BGLAP*-Cre) allele, hemizygous male Tg(*BGLAP*-Cre) mice were bred to female mice homozygous for the *R26*$^{l\text{-}s\text{-}lLacZ}$ allele. Tg(*BGLAP*-Cre);*R26*$^{l\text{-}s\text{-}lLacZ/+}$ and *R26*$^{l\text{-}s\text{-}lLacZ/+}$ littermate offspring were then euthanized at different postnatal ages, and their heads were sectioned coronally and stained for β-galactosidase activity. No CNS staining was observed in P0 mice (data not shown). At P14, the age when Tg(*BGLAP*-Cre);*Pik3ca*$^{H1047R/+}$ mice begin to appear different from their littermates, β-galactosidase activity was seen in granule cells of the dentate gyrus and in some CA3 pyramidal neurons of the hippocampus of Tg(*BGLAP*-Cre);*R26*$^{l\text{-}s\text{-}lLacZ/+}$ mice, and not in the corresponding regions of control mice (Figure 3A-F). This pattern of Tg(*BGLAP*-Cre)-mediated recombination in the hippocampus extends from its anterior to posterior region. Additionally, β-galactosidase activity was detected in the granular cells of the cerebellar gyri of Tg(*BGLAP*-Cre);*R26*$^{l\text{-}s\text{-}lLacZ/+}$ mice (Figure 3G - N)**.** Furthermore, the number of LacZ expressing cells in the cerebellar gyri appeared to increase as the animals aged (Figure 3K and M).

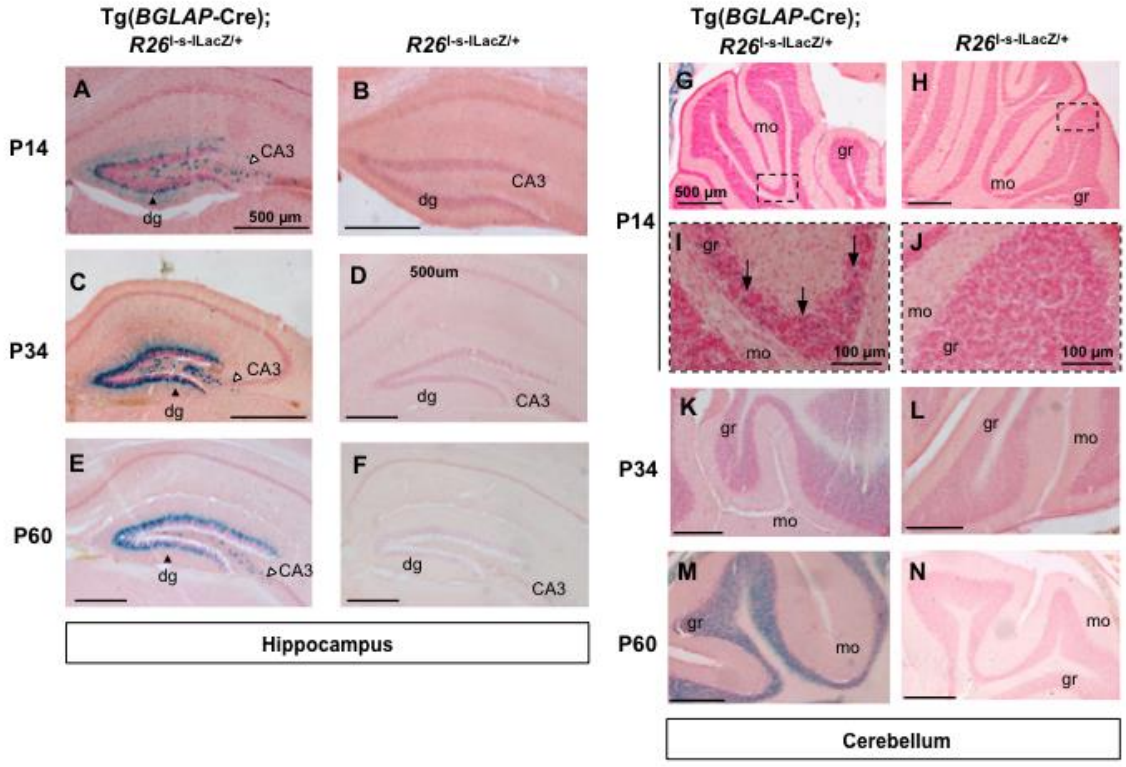

Figure 3. Tg(*BGLAP*-Cre) is active in mouse hippocampus and cerebellum. **(Left panels)** Photomicrographs of coronal sections through the hippocampi of P14, P34, and P60 Tg(*BGLAP*-Cre);*R26*$^{l\text{-}s\text{-}lLacZ/+}$ and *R26*$^{l\text{-}s\text{-}lLacZ/+}$ littermates. Each section is stained for β-galactosidase activity. Note LacZ expressing cells are present only in granule cells (black arrowheads) of the dentate gyrus (dg) and in CA3 pyramidal neurons (white arrowhead) of Tg(*BGLAP*-Cre);*R26*$^{l\text{-}s\text{-}lLacZ/+}$ mice. **(Right panels)** Photomicrographs of coronal sections through the cerebellums of P14, P34, and P60 Tg(*BGLAP*-Cre);*R26*$^{l\text{-}s\text{-}lLacZ/+}$ and *R26*$^{l\text{-}s\text{-}lLacZ/+}$ littermates. Each section is stained for β-galactosidase activity. Note only cells in the granular (gr) layer and not the molecular (mo) layer of the cerebellum express LacZ in Tg(*BGLAP*-Cre);*R26*$^{l\text{-}s\text{-}lLacZ/+}$ mice. Furthermore, the fraction of LacZ expressing cells in the cerebellar granular cells appears to increase with age. All scalebars are 500 µm, except for scalebars in panels I and J, which represent the boxed areas from panels I and H and are 100 µm.

To determine if Tg(*BGLAP*-Cre);*Pik3ca*$^{H1047R/+}$ mice had increased PI3K activity in Cre-recombined CNS cells, we performed immunohistochemistry using an anti-Phospho-mTOR antibody. At P18, compared to a *Pik3ca*$^{H1047R/+}$ littermate control, the Tg(*BGLAP*-Cre);*Pik3ca*$^{H1047R/+}$ mouse had increased Phospho-mTor immunoreactivity in many cerebellar granule cells (Supplementary Figure 6). Increased phospho-mTor immunoreactivity was also

observed in most calvarial bone cells from the Tg(*BGLAP*-Cre);*Pik3ca*$^{H1047R/+}$ mouse and not in the control littermate (Supplementary Figure 7).

Discussion

Tg(*BGLAP*-Cre) mice were generated more than a decade ago by cloning a 3.5 kb DNA human *BGLAP* regulatory element upstream of Cre-recombinase and injecting into fertilized eggs[9]. Tg(*BGLAP*-Cre) mice were generously donated to the Jackson Lab for public distribution and have been used in dozens of studies (https://www.jax.org/strain/019509) assessing the consequence of recombining loxP flanked (floxed) alleles in osteoblasts and osteocytes. Cell-type specific expression of the *BGLAP*-Cre transgene was inferred from northern blots looking for *Cre* mRNA expression, from Southern blots and PCR assays that looked for recombination of floxed alleles, and from fluorescence microscopy using reporter mouse strains (e.g.,[8,9,30]). However, these assays examined limited numbers of tissues and were insensitive to low levels of *Cre* expression or low levels of Cre-mediated recombination. Thus, data from these studies does not preclude Tg(*BGLAP*-Cre) being active at non-skeletal sites. Nevertheless, there remains a misconception that *BGLAP*-Cre expression is restricted to osteoblasts and osteocytes[30]. In contrast, expression we found outside of the skeletal system for Tg(*DMP1*-Cre), such as in muscle and brain, has previously been observed by us and other investigators[17,31-33].

In bone, in addition to osteoblasts and osteocytes, Tg(*BGLAP*-Cre) expression has been observed in arteriolar pericytes and Cxcl12-associated reticular cells[33]. Here we show that Tg(*BGLAP*-Cre) is also more broadly expressed, and we describe a ddPCR method to identify and quantify Cre-mediated recombination in tissues and cells. We suspected Tg(*BGLAP*-Cre) had “off-target" (i.e., non-bone) expression because Tg(*BGLAP*-Cre);*Pik3ca*$^{H1047R/+}$ mice developed profound lymphatic enlargement with hemorrhage overlying their skulls, failed to gain weight, and died by 7 weeks of age. After excluding bone-derived hematologic and metabolic

causes for the early lethality, we looked for activated PI3K signaling in other tissues that have been associated with deleterious effects in humans and mice. We utilized ddPCR[34], a powerful method for detecting low frequency somatic mutations, and found Tg(*BGLAP*-Cre)-mediated recombination in multiple tissues, including skin, brain, and muscle. Interestingly, Tg(*BGLAP*-Cre) expression appeared localized to specific brain regions such as hippocampus and cerebellum (Figure 3), and was not apparent at birth. Also, with respect to CNS expression of Tg(*BGLAP*-Cre), we observed comparable levels of Cre activity (Table 1) in mice having different floxed alleles (e.g., $R26^{mTmG}$ and $Prg4^{GT}$).

At present, we do not know why Tg(*BGLAP*-Cre);$Pik3ca^{H1047R/+}$ mice die and have a phenotype that is different from that of mice with Tg(*BGLAP*-Cre)-induced loss-of-function mutations in *Pten* [8]. Several possibilities may account for this difference. First, PIK3CA may signal via some pathways that are not regulated by PTEN. Second, PIK3CA activation requires recombination of only 1 allele, whereas PTEN inactivation requires recombination of 2 alleles. Third, mRNA transcripts encoding 2 other catalytic subunits of the PI3 kinase signaling pathway, PIK3CB and PIK3CD, are expressed in bone[15]; these subunits may be responsible for increasing bone mass in PTEN deficient mice and/or for mitigating the effects of PIK3CA over-activity. However, the similarity between Tg(*BGLAP*-Cre)-mediated PTEN loss-of-function and Tg(*DMP1*-Cre)-mediated PIK3CA gain-of-function mice, with regard to their survival and increased bone mass, suggests the difference in phenotype between the *Tg*(*BGLAP*-Cre) and Tg(*DMP1*-Cre) mice is due to their having non-overlapping extraskeletal sites of Cre-recombination. Large lymphatic malformations seen in Tg(*BGLAP*-Cre);$Pik3ca^{H1047R/+}$, and not in Tg(*DMP1*-Cre);$Pik3ca^{H1047R/+}$, mice may be responsible for the former animals' early lethality, since similar malformations can be debilitating and deadly in humans[35].

We do not know whether Tg(*BGLAP*-Cre) expression in the brain reflects endogenous sites of osteocalcin production, ectopic transgene expression due to sequences in the transgene itself, or ectopic transgene expression due to the site of transgene integration. *BGLAP*

transcripts are present in human brain RNA-sequencing data (https://www.gtexportal.org/home/gene/BGLAP), and *Bglap* expression has also been reported in rat brain[36]. Mice have three *Bglap* paralogs located on chromosome 3[37]. Two paralogs are highly expressed in bone, while the third is not expressed in bone but is expressed in other tissues including brain[37]. *In situ* hybridization studies reveal expression of at least one *Bglap* paralog in mouse brain (http://mouse.brain-map.org/gene/show/11881).

Regardless of the mechanism(s) responsible for determining where Tg(*BGLAP*-Cre) is expressed, our data indicate this transgene is not bone-specific. Therefore, investigators should consider off-target sites of Cre-recombinase activity when interpreting, or re-interpreting, data that have been generated with these mice. Many strains of Cre-driver mice have unanticipated sites of Cre-expression, and mice with inducible Cre-recombinase activity (e.g., Tet-On and tamoxifen-inducible systems) can become active without induction (i.e., leakiness)[38]. Furthermore, an animal's genetic background and the floxed allele being recombined can also influence Cre-recombinase expression, leakiness, or efficiency. Similar considerations apply to mice that express Flp-recombinase.

Several methods are available to detect unanticipated sites of Flp- or Cre- activity and to quantify rates of recombination, including using mice with fluorescent or enzymatic reporters that can be assessed by microscopic imaging, or performing quantitative PCR using allele specific fluorescent reporter probes. We prefer using ddPCR. Although the fluorescent reporter probe cost is identical to that of quantitative PCR, we find ddPCR assays are simple to set up, sensitive, and specific. Advantages of performing ddPCR before using mouse strains with fluorescent or enzymatic reporter alleles, are the ability of ddPCR to quantify recombination rates for any allele of interest, not just the reporter allele, and to detect low levels of recombination that may be missed if a histologically examined section didn't include the region of a tissue that contains recombined cells. We were conservative in considering recombination

frequencies < 0.5% as potentially representing false positive results based on our prior work with other ddPCR assays[1]. However, the assays described herein are highly specific, suggesting the threshold for detecting true recombination, particularly for commonly used reporter alleles, such as *R26*^{mTmG}, is much lower. It is also important to recognize that we found differences in recombination frequency when the same tissue was recovered from animals with the same genotype (Table 1). We suspect these differences reflect sampling variation between animals since each tissue is actually comprised of multiple cell types for which only a subset of cells may contain recombined alleles; however, we cannot preclude the differences we observed among genetically matched animals being true biologic variation. With ddPCR it becomes possible to quantify recombination in multiple tissues/sites using DNA derived from thousands of cells in each tissue. Furthermore, ddPCR can be used on DNA recovered from formalin fixed tissues and histologic sections, enabling analysis of experiments in which samples have been archived. When unexpected Cre or Flp recombination occurs, fluorescence and histochemical methods can then be employed to determine the identities of the recombined cells.

Acknowledgements

The authors thank Dr. Wayne Phillips for providing *Pik3ca*^{H1047R} mice, Dr. Julia Charles and Ms. Evelyn Flynn for sharing technical expertise, and the Animal Care Resources at Children's Hospital (ARCH) staff for performing complete blood counts and serum biochemical analyses. This work was supported by NIH/NIAMS grants AR-64231 and AR-53237.

References

1. Luks VL, Kamitaki N, Vivero MP, Uller W, Rab R, Bovee JV, et al. Lymphatic and other vascular malformative/overgrowth disorders are caused by somatic mutations in PIK3CA. The Journal of pediatrics. Apr 2015;166(4):1048-54 e1-5.

2. Kurek KC, Luks VL, Ayturk UM, Alomari AI, Fishman SJ, Spencer SA, et al. Somatic mosaic activating mutations in PIK3CA cause CLOVES syndrome. American journal of human genetics. Jun 08 2012;90(6):1108-15.
3. Vanhaesebroeck B, Whitehead MA, Pineiro R. Molecules in medicine mini-review: isoforms of PI3K in biology and disease. Journal of molecular medicine. Jan 2016;94(1):5-11.
4. Fresno Vara JA, Casado E, de Castro J, Cejas P, Belda-Iniesta C, Gonzalez-Baron M. PI3K/Akt signalling pathway and cancer. Cancer treatment reviews. Apr 2004;30(2):193-204.
5. Sun H, Lesche R, Li DM, Liliental J, Zhang H, Gao J, et al. PTEN modulates cell cycle progression and cell survival by regulating phosphatidylinositol 3,4,5,-trisphosphate and Akt/protein kinase B signaling pathway. Proceedings of the National Academy of Sciences of the United States of America. May 25 1999;96(11):6199-204.
6. Sapp JC, Turner JT, van de Kamp JM, van Dijk FS, Lowry RB, Biesecker LG. Newly delineated syndrome of congenital lipomatous overgrowth, vascular malformations, and epidermal nevi (CLOVE syndrome) in seven patients. American journal of medical genetics Part A. Dec 15 2007;143A(24):2944-58.
7. Alomari AI. Characterization of a distinct syndrome that associates complex truncal overgrowth, vascular, and acral anomalies: a descriptive study of 18 cases of CLOVES syndrome. Clinical dysmorphology. Jan 2009;18(1):1-7.
8. Liu X, Bruxvoort KJ, Zylstra CR, Liu J, Cichowski R, Faugere MC, et al. Lifelong accumulation of bone in mice lacking Pten in osteoblasts. Proceedings of the National Academy of Sciences of the United States of America. Feb 13 2007;104(7):2259-64.
9. Zhang M, Xuan S, Bouxsein ML, von Stechow D, Akeno N, Faugere MC, et al. Osteoblast-specific knockout of the insulin-like growth factor (IGF) receptor gene reveals an essential role of IGF signaling in bone matrix mineralization. The Journal of biological chemistry. Nov 15 2002;277(46):44005-12.
10. Lu Y, Xie Y, Zhang S, Dusevich V, Bonewald LF, Feng JQ. DMP1-targeted Cre expression in odontoblasts and osteocytes. Journal of dental research. Apr 2007;86(4):320-5.
11. Muzumdar MD, Tasic B, Miyamichi K, Li L, Luo L. A global double-fluorescent Cre reporter mouse. Genesis. Sep 2007;45(9):593-605.
12. Soriano P. Generalized lacZ expression with the ROSA26 Cre reporter strain. Nature genetics. Jan 1999;21(1):70-1.
13. Kinross KM, Montgomery KG, Kleinschmidt M, Waring P, Ivetac I, Tikoo A, et al. An activating Pik3ca mutation coupled with Pten loss is sufficient to initiate ovarian tumorigenesis in mice. The Journal of clinical investigation. Feb 2012;122(2):553-7.
14. Hill A, Waller KA, Cui Y, Allen JM, Smits P, Zhang LX, et al. Lubricin restoration in a mouse model of congenital deficiency. Arthritis & rheumatology. Nov 2015;67(11):3070-81.
15. Kedlaya R, Veera S, Horan DJ, Moss RE, Ayturk UM, Jacobsen CM, et al. Sclerostin inhibition reverses skeletal fragility in an Lrp5-deficient mouse model of OPPG syndrome. Science translational medicine. Nov 13 2013;5(211):211ra158.
16. Dempster DW, Compston JE, Drezner MK, Glorieux FH, Kanis JA, Malluche H, et al. Standardized nomenclature, symbols, and units for bone histomorphometry: a 2012 update of the report of the ASBMR Histomorphometry Nomenclature Committee. Journal of bone and mineral research : the official journal of the American Society for Bone and Mineral Research. Jan 2013;28(1):2-17.
17. Cui Y, Niziolek PJ, MacDonald BT, Zylstra CR, Alenina N, Robinson DR, et al. Lrp5 functions in bone to regulate bone mass. Nature medicine. Jun 2011;17(6):684-91.
18. Asada N, Katayama Y. Regulation of hematopoiesis in endosteal microenvironments. International journal of hematology. Jun 2014;99(6):679-84.
19. Calvi LM. Osteolineage cells and regulation of the hematopoietic stem cell. Best practice & research Clinical haematology. Sep 2013;26(3):249-52.

20. Morrison SJ, Scadden DT. The bone marrow niche for haematopoietic stem cells. Nature. Jan 16 2014;505(7483):327-34.
21. Bonewald LF. The Role of the Osteocyte in Bone and Nonbone Disease. Endocrinology and metabolism clinics of North America. Mar 2017;46(1):1-18.
22. Sato M, Katayama Y. Osteocytes and Homeostasis of Remote Organs : Bone-Buried Osteocytes Talk to Remote Organs. Current osteoporosis reports. Aug 2015;13(4):193-7.
23. Castillo SD, Tzouanacou E, Zaw-Thin M, Berenjeno IM, Parker VE, Chivite I, et al. Somatic activating mutations in Pik3ca cause sporadic venous malformations in mice and humans. Science translational medicine. Mar 30 2016;8(332):332ra43.
24. Osborn AJ, Dickie P, Neilson DE, Glaser K, Lynch KA, Gupta A, et al. Activating PIK3CA alleles and lymphangiogenic phenotype of lymphatic endothelial cells isolated from lymphatic malformations. Human molecular genetics. Feb 15 2015;24(4):926-38.
25. Roy A, Skibo J, Kalume F, Ni J, Rankin S, Lu Y, et al. Mouse models of human PIK3CA-related brain overgrowth have acutely treatable epilepsy. eLife. Dec 03 2015;4.
26. Kinross KM, Montgomery KG, Mangiafico SP, Hare LM, Kleinschmidt M, Bywater MJ, et al. Ubiquitous expression of the Pik3caH1047R mutation promotes hypoglycemia, hypoinsulinemia, and organomegaly. FASEB journal : official publication of the Federation of American Societies for Experimental Biology. Apr 2015;29(4):1426-34.
27. Ayturk UM, Couto JA, Hann S, Mulliken JB, Williams KL, Huang AY, et al. Somatic Activating Mutations in GNAQ and GNA11 Are Associated with Congenital Hemangioma. American journal of human genetics. Apr 07 2016;98(4):789-95.
28. Couto JA, Huang AY, Konczyk DJ, Goss JA, Fishman SJ, Mulliken JB, et al. Somatic MAP2K1 Mutations Are Associated with Extracranial Arteriovenous Malformation. American journal of human genetics. Mar 02 2017;100(3):546-54.
29. Forbes SA, Beare D, Boutselakis H, Bamford S, Bindal N, Tate J, et al. COSMIC: somatic cancer genetics at high-resolution. Nucleic acids research. Jan 04 2017;45(D1):D777-D83.
30. Mosialou I, Shikhel S, Liu JM, Maurizi A, Luo N, He Z, et al. MC4R-dependent suppression of appetite by bone-derived lipocalin 2. Nature. Mar 16 2017;543(7645):385-90.
31. Kalajzic I, Matthews BG, Torreggiani E, Harris MA, Divieti Pajevic P, Harris SE. In vitro and in vivo approaches to study osteocyte biology. Bone. Jun 2013;54(2):296-306.
32. Lim J, Burclaff J, He G, Mills JC, Long F. Unintended targeting of Dmp1-Cre reveals a critical role for Bmpr1a signaling in the gastrointestinal mesenchyme of adult mice. Bone research. 2017;5:16049.
33. Zhang J, Link DC. Targeting of Mesenchymal Stromal Cells by Cre-Recombinase Transgenes Commonly Used to Target Osteoblast Lineage Cells. Journal of bone and mineral research : the official journal of the American Society for Bone and Mineral Research. Nov 2016;31(11):2001-7.
34. Hindson BJ, Ness KD, Masquelier DA, Belgrader P, Heredia NJ, Makarewicz AJ, et al. High-throughput droplet digital PCR system for absolute quantitation of DNA copy number. Analytical chemistry. Nov 15 2011;83(22):8604-10.
35. Trenor CC, 3rd, Chaudry G. Complex lymphatic anomalies. Seminars in pediatric surgery. Aug 2014;23(4):186-90.
36. Fleet JC, Hock JM. Identification of osteocalcin mRNA in nonosteoid tissue of rats and humans by reverse transcription-polymerase chain reaction. Journal of bone and mineral research : the official journal of the American Society for Bone and Mineral Research. Oct 1994;9(10):1565-73.
37. Desbois C, Hogue DA, Karsenty G. The mouse osteocalcin gene cluster contains three genes with two separate spatial and temporal patterns of expression. The Journal of biological chemistry. Jan 14 1994;269(2):1183-90.

38. Heffner CS, Herbert Pratt C, Babiuk RP, Sharma Y, Rockwood SF, Donahue LR, et al. Supporting conditional mouse mutagenesis with a comprehensive cre characterization resource. Nature communications. 2012;3:1218.

Credit Author Statement

K.D. and M.L.W. conceived and designed the experiments. All co-authors performed experiments and interpreted data. K.D., S.L., and M.L.W. wrote an initial draft of the manuscript. All co-authors contributed figures, wrote and revised the manuscript, and approved the submitted version.

Highlights

- *BGLAP*-Cre and *DMP1*-Cre transgenes are expressed in unexpected locations in mice.
- Off-target recombination can confound interpretation of data using these transgenes.
- ddPCR detects and quantifies allele-specific, off-target recombination events.